Importance of austenitization temperature and ausforming on creep strength in 9Cr ferritic/martensitic steel

Vivas, J.; Capdevila, C.; Altstadt, E.; Houska, M.; San-Martin, D.;

Originally published:

May 2018

Scripta Materialia 153(2018), 14-18

DOI: https://doi.org/10.1016/j.scriptamat.2018.04.038

Perma-Link to Publication Repository of HZDR:

https://www.hzdr.de/publications/Publ-27383

Importance of austenitization temperature and ausforming on Creep strength in 9Cr ferritic/martensitic steel

J. Vivas[1*], C. Capdevila[1], E. Altstadt[2], M. Houska[2], D. San-Martín[1]

[1]Materalia Research Group, Physical Metallurgy Department, Centro Nacional de Investigaciones Metalúrgicas (CENIM-CSIC), Avda. Gregorio del Amo 8, 28040 Madrid, Spain.

[2] Helmholtz-Zentrum Dresden - Rossendorf (HZDR), Bautzner Landstraße 400, 01328 Dresden, Germany

*Corresponding author.

E-mail address : jvm@cenim.csic.es (J.Vivas)

Abstract

Small Punch Creep technique was used as a screening procedure to evaluate the creep properties of different microstructures developed in a thermomechanical simulator. The goal seek was to generate alternative microstructures in a conventional ferritic-martensitic G91 steel grade which boost thermal stability at temperatures as high as 700 ºC. The developed microstructures allow studying the effect of the austenitization temperature optimized by thermodynamic calculations and the ausforming on the creep strength and ductility. The improvement in creep strength recorded was attributable to a higher number density of MX precipitates. By contrast, these microstructures showed an important reduction in creep ductility.

Keywords: Small Punch Creep Tests; MX nanoprecipitates; creep ductility; ausforming; creep resistant steels

The need to look for ways to ensure the sustainability of current energy sources to guarantee the viability of future generations, as long as they are environmentally friendly, is beyond dispute. The future of the power plant is to reduce fuel costs and

CO_2 emissions thought improvements in efficiency by elevating steam conditions to even higher ranges of pressure and temperature. The increase in thermal efficiency has been the driving force to develop new generations of 9 wt. % Cr Ferritic/Martensitic (FM) steels for structural applications [1-3]. Heat resistant steels used for high temperature component in power plants must have good mechanical properties, fabricability, corrosion resistant and creep strength. This last property is the most important feature and it has led innumerable research activities aiming at improving the creep strength in alloy development.

The creep resistant FM steels derive their creep strength from four principal sources, such as solid-solution strengthening, dislocation substructures, $M_{23}C_6$ precipitation at prior austenite grains, block and lath boundaries, and the intra- and intergranular distribution of MX nanosized precipitates. There are basically two ways to optimize all those four parameters. One way is by optimizing the steel chemistry. This idea has been developed along all history of heat resistant steels [4, 5]. The first 9Cr-1Mo, known as zero generation, contained mainly 9wt. % Cr for improvement in corrosion resistance. First generation added V and Nb to enhance precipitate strengthening. In the second generation, N was added and the amount of C, V and Nb was optimized to improve precipitate strengthening. In the third generation some of the Mo added in previous generation to improve solid solution strengthening was substituted by W. Furthermore, B was added in these steels to avoid microstructural degradation [6, 7]. Finally, the actual generation is focused on pushing operation temperature up to 700 ºC. For this purpose, the chemistry of the steel contains higher amount of W than previous generations to increase solid solution strengthening. However, W is a ferrite-stabilizer that triggers δ-ferrite formation. This fact leads to the addition up to 3 wt. % Co in order to avoid δ-ferrite formation since this phase deteriorates creep properties by inhomogeneous deformation [8-10]. At the end of the day, the development of new alloying compositions implies the use of very expensive elements such as W and Co that increase the cost of the steel. Thus, other way to improve creep strength should be considered.

An alternative strategy consists in applying a combination of non conventional thermomechanical treatments to obtain the most adequate microstructure in order to guarantee the best creep response at elevated temperature of the steel [11-15]. The purpose of this work is to explore this alternative route in conventional heat-resistant

steel such as G91. The chemical composition of the G91 steels used in this work is Fe-8.76Cr-0.088C-0.317Si-0.597Mn-0.862Mo-0.186V-0.073Nb.Two alternative processing routes are considered:

- Higher Austenitization Temperature (HAT). Higher austenitization temperature will be used to achieve an almost complete solid solution in austenite of MX precipitate formers. Therefore, higher number density of MX precipitates will be achieved during subsequent tempering.
- Thermomechanical Treatment (TMT). In this treatment, the combined effect of the increase in the austenitization temperature and deformation will be studied with the aim of optimizing the MX-nanoprecipitates distribution, and the microstructure of the martensitic matrix.

Figure 1 schematically illustrates these two non conventional heat treatments (TMT and HAT). The simulations were carried out on 10 mm in length and 8 mm in diameter cylindrical samples using a 805 DIL Bahr plastodilatometer. The samples were heated at 5 ºC/s and cooled at 50 ºC/s. The deformation applied in the thermomechanical treatment was 40 % at 0.1 s^{-1} and the deformation temperature was 900 ºC. For the sake of comparison, Fig. 1 also includes the industrial manufacturing conditions for G91 steel named as-received (AR) condition. The microstructure in the AR condition after austenitization (1040 ºC) consists in highly dislocated martensite laths and some precipitates that do not dissolve during austenitization (primary precipitates).

The most important characteristic to get better high-temperature creep strength is to achieve a good microstructural stability at the corresponding operating temperature. The loss of creep rupture strength in G91 is due to the recovery of the martensitic lath microstructure because of the dislocation movement [16, 17]. The dislocation pinning by nanosized MX precipitates can delay this phenomenon, since they present better ripening resistance than $M_{23}C_6$ carbides [18-21]. The goal of undergoing such elevated temperatures in the HAT treatment as compared to conventional austenitization heat treatment (AR treatment) is to eliminate as many as possible primary carbides formed during the casting process. It is important to consider that the austenitization temperature has to be lower than the temperature for delta ferrite formation in order to avoid this phase since it is detrimental from long-term creep properties point of view. Computational thermodynamic calculations by means of Thermocalc® determine the

optimum austenitization temperature in 1225ºC. Therefore, the martensite formed after quenching from such elevated austenitization temperature keeps in solid solution most precursor elements of MX carbides that might precipitate during subsequent tempering.

Regarding the TMT treatment, it has been reported in literature the role of austenite deformation on refining the martensitic microstructure [22, 23]. Depending on the deformation temperature, several are the microstructural features that change in the austenite and could be transferred to the martensite upon quenching. Deformation temperatures above the austenite recrystallization temperature can produce an austenite grain refinement that can induce the concomitant martensitic microstructural refinement. Similarly, by applying plastic deformation prior to the martensite transformation below recrystallization temperature, which is called ausforming [24], deformation bands in the austenite can be generated, which directly induce that some specific variants are formed preferentially, leading to development of a strong transformation texture selection (martensite variant selection) and anisotropic properties.

Figure 2 illustrates the IPF maps, SEM and TEM micrographs after HAT and TMT processing routes and the reference (AR) condition. It is clear from the comparison that the elevated austenitization temperatures achieved in HAT and TMT routes induce a considerably block coarsening in the martensitic microstructure. The IPF maps shown in Fig. 2 consist of a tempered martensite microstructure with a typical plate-like morphology of martensite. Block widths were measured by the linear intercept method [25]. Boundaries with a misorientation larger than 10º were considered as block boundaries in the EBSD maps (example of a characteristic block has been indicated with arrows). The corresponding block widths are 2.7±0.2 μm for AR condition, 4.12±0.37 μm for HAT and 3.21±0.27 μm for TMT. The coarser prior austenite grain achieved after the high austenitization temperature induces such differences in block size. The coarser the prior austenite grain, the coarser the block size. This is consistent with the fact that thermomechanical processing increases the low angle substructure and decreases the block size of as-quenched martensite. The dislocation density after HAT and TMT was measured by XRD using Co-Kα radiation in a Bruker AXS D8 diffractometer equipped with Goebel mirror optics and a LynxEye Linear Position Sensitive Detector. The results show a dislocation density of $14\pm0.1\cdot10^{14}$ m^{-2} and $22\pm0.1\cdot10^{14}$ m^{-2} after austenitization and ausforming, respectively. This result confirms

the increase in dislocation density in as-quenched martensite after TMT. Similar effect of ausforming on dislocation density was reported by other authors [26, 27]. Finally, TEM examination of the microstructure allowed us to determine the lath width of the martensitic microstructure by the linear intercept method. Values of 360±35 nm for AR condition, 350±20 nm for HAT condition, and 318±32 nm for TMT condition were obtained.

Another particular feature of tempered martensitic microstructures is the distribution of $M_{23}C_6$ precipitates. Figure 2 illustrates the distribution of $M_{23}C_6$ carbides after AR, HAT and TMT processing routes. Relatively large, about 70 to 500 nm, closely spaced $M_{23}C_6$ carbides were observed. The number density and average particle size of these carbides were calculated through SEM micrographs to be 6.19×10^{19} m^{-3} and 141±3 nm for AR condition, 8.24×10^{19} m^{-3} and 124±3 nm for HAT condition, and 4.11×10^{19} m^{-3} and 143±5 nm for TMT steel. These values are very similar to those reported by Klueh et al. for the steel after conventional heat treatment [28].

The finely disperse MX nanoprecipitates present in this microstructures were revealed inside the laths (Fig. 2) and associated with dislocations, which suggests the role of dislocations as potential nucleation sites for MX nanoprecipitates, and proves the importance of ausforming in generating a microstructure where nanosized MX particles are more homogeneously distributed. These spherical MX nanoprecipitates had a mean particle size of 12±1 nm with a number density of 7.20×10^{21} m^{-3} for HAT steel and 9±1 nm with a number density of 1.86×10^{22} m^{-3} for TMT steel. The MX precipitates are, in both cases, significantly smaller than those measured in the AR condition, i.e. a particle size of 25±5 nm with a number density of 8.14×10^{19} m^{-3}. The size values obtained after HAT and TMT are smaller, and the number density higher, as compared to measurements reported in the literature after conventional heat treatments [29].

So far, the differences observed in the microstructure after the AR, HAT and TMT conditions could be summarized as follows. After the conventional processing route (AR condition), the tempered martensite microstructure presents finer block width but coarser lath width than both HAT and TMT processing routes. However, as mentioned above, the key to develop an optimized treatment to improve the creep strength of G91 is to produce a dispersion of thermally stable nanosized MX precipitates able to pin

dislocations at high temperature, and hence, retard microstructure degradation. The strategy followed in this work is two-fold. First, the steel underwent an austenitization temperature as high as 1225 ºC. Thus, the majority of MX carbide formers were in solid solution in austenite. Secondly, an ausforming procedure was added. The ausforming target was to boost the number density of MX precipitates by increasing the potential nucleation sites. Nucleation sites are introduced in form of dislocation by hot working. The dislocations produced in austenite would be inherited by martensite or would modify the martensitic transformation producing an increase in the dislocations density of fresh martensite and a finer precipitation after subsequent tempering. This is consistent with the higher dislocation density determined for TMT as compared with HAT condition, as well as the higher number density for nanosized MX precipitates measured after TMT processing route.

The creep response of the AR, HAT and TMT conditions is evaluated through small punch creep tests (SPCT). Description of this technique is found elsewhere [26, 30-34]. The output of small punch creep tests, disc deflection vs time, is divided in three regions. These regions are similar to the strain versus time curves obtained from uniaxial creep tests, however in SP creep tests the failure in ductile materials occurs away from the load line with cracks propagating in a circumferential direction due to membrane stretching. There is, therefore, an initial loading region where the spherical indenter loads on a very small contact area of the sample. Since the stresses will be higher than the yield stress of the material, local plasticity and an initial large deformation is produced. This large deformation is accumulated in a short time. The second stage is the steady state region. In this region the disk deflection rate is almost a stationary minimum. This region is most of the sample life. Finally, the third stage consists in an acceleration and fracture region. A possible explanation of this behavior is that, after a crack propagates to a critical length the sample is no longer in balance, leading to an increase in deflection rate and to a reduction in the structure stiffness in the tertiary region. Another explanation is based on the localized necking without crack presence. The deformation mechanism in the tertiary region is a mixture among accumulation of creep damage, geometric softening and crack growth effect.

Figure 3a) shows the disc deflection versus time curves obtained for the three conditions studied (AR, HAT and TMT) at 700 ºC with a load of 200 N. One might conclude from the figure that the creep strength was significantly improved after TMT condition. The

time to rupture was 2.5 and 1.24 times greater than AR condition, from 38 hours to 95 and 48 hours for the TMT and HAT, respectively. The minimum disk deflection rate was 2.9 $\mu m \cdot h^{-1}$ for the TMT sample while for the HAT sample was 3.7 $\mu m \cdot h^{-1}$. These minimum disk deflections rates were significantly slower than the minimum disk deflection rate measured for the G91 in the AR condition, which was 9.5 $\mu m \cdot h^{-1}$. The results obtained suggest that the increase in the number density of MX precipitates strengthens at high temperature, since they are able to pin more effectively the dislocations. Hence, this phenomenon reduces minimum creep rate and retards the onset of the tertiary creep. The differences in minimum disk deflection rate and time to rupture between the sample after TMT and HAT discloses the importance of ausforming. Taking into account the similar number density of MX nanoprecipitates and the similar minimum disk deflection rate obtained for the TMT and HAT, the great differences in time to rupture are explained base on the higher creep damage tolerance for the TMT. As it has been reported in other works the creep damage tolerance is influenced by the prior austenite grain size (PAGS) in ferritic/martensitic steels [35]. By increasing the prior austenite grain size the creep damage tolerance is reduced, which could even produce a change in creep fracture behavior accompanied with a drop in ductility. This is consistent with the PAGSs values achieved, i.e. 250±7 μm and 128±17 μm for HAT and TMT conditions, respectively. The partial dynamic recrystallization of the austenite during ausforming at 900 ºC, bearing in mind that the non-recrystallization temperature of this steel might be below 880 ºC, refines the prior austenite grain size and increases the creep damage tolerance extending the tertiary creep stage and, in consequence, the time to rupture. The fact that the TMT sample overruns the values achieved by the HAT sample, reveals the goodness of the optimized thermomechanical processing to improve the creep strength of G91 steel. The duration of the SPCTs is below 100 hours and, therefore, they are strongly influenced by the initial microstructures. As it has been reported previously [36] for short time creep tests, dislocation strengthening contributes to increase time to rupture; by contrast, this hardening is not useful during long term creep tests because the high dislocation density promotes the recovery and the recrystallization. As it can be seen in figure 2, a higher dislocation density has been observed in the TMT sample compared to HAT sample. Hence, the improved creep strength could be supported by the high dislocation density and not just by the higher number density of MX nanoprecipitates. As Maruyama et al.

postulated in their work [37]: “a material with high dislocation density is useless unless its premature recovery of dislocation substructure is prevented by some means”. In this case the means to avoid the premature recovery of dislocations would be the MX nanoprecipitates. These precipitates would extend the strengthening contribution of the dislocation to longer times, improving the creep strength for the TMT condition not only because of the better distribution of MX, but also because it prolongs the strengthening contribution of the dislocations. Conventional long-term creep tests should be done to clarify this hypothesis.

It is important to mention that the images in Fig. 3 b), c) and d) suggest that the reduction in thickness after SPCT for HAT and TMT conditions was considerably smaller than for the AR condition. However, these observations are not conclusive because the curves show the displacement of the punch ball. Theses curves terminate when the ball is completely pushed through the disc (Fig. 3 b-d). This stage is not identical with the onset of the macroscopic cracking. It is more appropriate to use the onset of the tertiary creep stage (i.e. the displacement at minimum displacement rate) to compare the creep deformation of the different samples (Fig. 3 a). Then, the creep deformation is much larger for G91-AR as compared to the other conditions. This is in line with a more pronounced thickness reduction of G91-AR. The reduction in thickness would suggest that an increment in the austenitization temperature produces an important drop in ductility [38].

In future publications the fracture behaviour and the microestructural degradation during creep tests will be studied in detail to explain this reduction in ductility.

Based on these facts, one might conclude that the martensitic microstructure achieved after TMT treatment should display superior creep behavior compared with those with a scarcer distribution of these particles, such as in the HAT and AR conditions. In this sense, the combination of an increasing austenitization temperature from 1040 to 1225 ºC and an ausforming processing at 900 ºC allow increasing the number density of MX up to 3 orders of magnitude which raises the strengthening capability of MX at 700 ºC. Ausforming increases the dislocation density after cooling and these dislocations act as nucleation sites for MX precipitates promoting higher number density of these. These microstructures reduce considerably the minimum disk deflection rate and show greater

time to rupture during SPCT carried out at 700 ºC. By contrast, such elevated austenitization temperature induces an important drop in ductility.

Acknowledgements

Authors acknowledge financial support to Spanish Ministerio de Economia y Competitividad (MINECO) through in the form of a Coordinate Project (MAT2016-80875-C3-1-R). The authors are grateful for the dilatometer tests by Phase Transformation laboratory. J. Vivas acknowledges financial support in the form of a FPI Grant BES-2014-069863. This work contributes to the Joint Programme on Nuclear Materials (JPNM) of the European Energy Research Alliance (EERA).

References

[1] R.L. Klueh, D.S. Gelles, S. Jitsukawa, A. Kimura, G.R. Odette, B. van der Schaaf, M. Victoria, Journal of Nuclear Materials 307–311, Part 1(0) (2002) 455-465.
[2] S.J. Zinkle, G.S. Was, Acta Materialia 61(3) (2013) 735-758.
[3] R.L. Klueh, A.T. Nelson, Journal of Nuclear Materials 371(1–3) (2007) 37-52.
[4] R.L. Klueh, K. Ehrlich, F. Abe, Journal of Nuclear Materials 191–194, Part A(0) (1992) 116-124.
[5] F. Masuyama, ISIJ International 41(6) (2001) 612-625.
[6] F. Abe, Procedia Engineering 10 (2011) 94-99.
[7] M.I.a.u.A. Toshiaki HORIUCHl.
[8] L. Helis, Y. Toda, T. Hara, H. Miyazaki, F. Abe, Materials Science and Engineering: A 510–511 (2009) 88-94.
[9] K. Sawada, M. Takeda, K. Maruyama, R. Ishii, M. Yamada, Y. Nagae, R. Komine, Materials Science and Engineering: A 267(1) (1999) 19-25.
[10] A. Kipelova, R. Kaibyshev, A. Belyakov, D. Molodov, Materials Science and Engineering: A 528(3) (2011) 1280-1286.
[11] R.L. Klueh, N. Hashimoto, P.J. Maziasz, Scripta Materialia 53(3) (2005) 275-280.

[12] S. Hollner, B. Fournier, J. Le Pendu, T. Cozzika, I. Tournié, J.C. Brachet, A. Pineau, Journal of Nuclear Materials 405(2) (2010) 101-108.
[13] L. Tan, J.T. Busby, P.J. Maziasz, Y. Yamamoto, Journal of Nuclear Materials 441(1–3) (2013) 713-717.
[14] L. Tan, Y. Yang, J.T. Busby, Journal of Nuclear Materials 442(1–3, Supplement 1) (2013) S13-S17.
[15] J. Vivas, C. Celada-Casero, D. San Martín, M. Serrano, E. Urones-Garrote, P. Adeva, M.M. Aranda, C. Capdevila, Metallurgical and Materials Transactions A 47(11) (2016) 5344-5351.
[16] F. Abe, Materials Science and Engineering: A 387 (2004) 565-569.
[17] F. Abe, S. Nakazawa, H. Araki, T. Noda, Metallurgical Transactions A 23(2) (1992) 469-477.
[18] F. Abe, M. Taneike, K. Sawada, International Journal of Pressure Vessels and Piping 84(1–2) (2007) 3-12.
[19] F. Abe, Materials Science and Engineering: A 319–321 (2001) 770-773.
[20] F. Abe, Current Opinion in Solid State and Materials Science 8(3–4) (2004) 305-311.
[21] M. Taneike, F. Abe, K. Sawada, Nature 424(6946) (2003) 294-296.
[22] T. Chiba, G. Miyamoto, T. Furuhara, Scripta Materialia 67(4) (2012) 324-327.
[23] G. Miyamoto, N. Iwata, N. Takayama, T. Furuhara, Acta Materialia 58(19) (2010) 6393-6403.
[24] I. Tamura, K. Tsuzaki, T. Maki, MORPHOLOGY OF LATH MARTENSITE FORMED FROM DEFORMED AUSTENITE IN 18% Ni MARAGING STEEL, Journal de Physique (Paris), Colloque, 1982, pp. c4. 551-c4. 556.
[25] C. Wang, M. Wang, J. Shi, W. Hui, H. Dong, Scripta Materialia 58(6) (2008) 492-495.
[26] D.J. Brookfield, W. Li, B. Rodgers, J.E. Mottershead, T.K. Hellen, J. Jarvis, R. Lohr, R. Howard-Hildige, A. Carlton, M. Whelan, The Journal of Strain Analysis for Engineering Design 34(6) (1999) 423-436.
[27] S.C. Kennett, STRENGTHENING AND TOUGHENING MECHANISMS IN LOW-C MICROALLOYED MARTENSITIC STEEL AS INFLUENCED BY AUSTENITE CONDITIONING, Department of Metallurgical and Materials Engineering, Colorado School of Mines, Golden, CO, USA, 2014.

[28] R.L. Klueh, N. Hashimoto, P.J. Maziasz, Journal of Nuclear Materials 367–370, Part A(0) (2007) 48-53.
[29] L. Tan, L.L. Snead, Y. Katoh, Journal of Nuclear Materials 478 (2016) 42-49.
[30] E.N. Campitelli, P. Spätig, R. Bonadé, W. Hoffelner, M. Victoria, Journal of Nuclear Materials 335(3) (2004) 366-378.
[31] Y. Ruan, P. Spätig, M. Victoria, Journal of Nuclear Materials 307(Part 1) (2002) 236-239.
[32] M.P. Manahan, A.S. Argon, O.K. Harling, Journal of Nuclear Materials 104(Supplement C) (1981) 1545-1550.
[33] E. Altstadt, H.E. Ge, V. Kuksenko, M. Serrano, M. Houska, M. Lasan, M. Bruchhausen, J.M. Lapetite, Y. Dai, Journal of Nuclear Materials.
[34] E. Altstadt, M. Serrano, M. Houska, A. García-Junceda, Materials Science and Engineering: A 654 (2016) 309-316.
[35] E. Plesiutschnig, C. Beal, C. Sommitsch, S. Paul, G. Zeiler, Scripta Materialia 122 (2016) 98-101.
[36] A. Iseda, H. Teranishi, F. Masuyama, Tetsu-to-Hagane 76(7) (1990) 1076-1083.
[37] K. Maruyama, K. Sawada, J.-i. Koike, ISIJ International 41(6) (2001) 641-653.
[38] E. Plesiutschnig, C. Beal, S. Paul, G. Zeiler, C. Sommitsch, Materials at High Temperatures 32(3) (2015) 318-322.

Figures

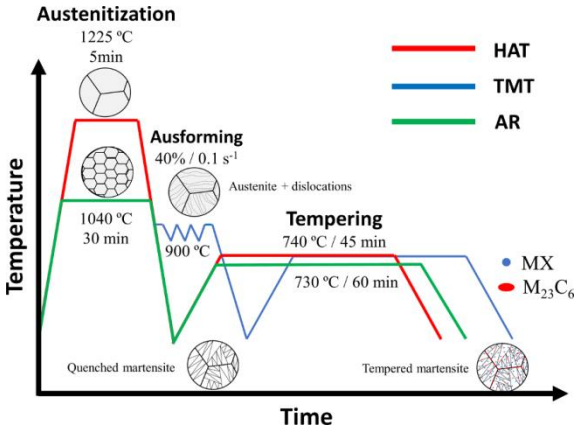

Figure 1. Scheme of the different thermomechanical and heat treatments

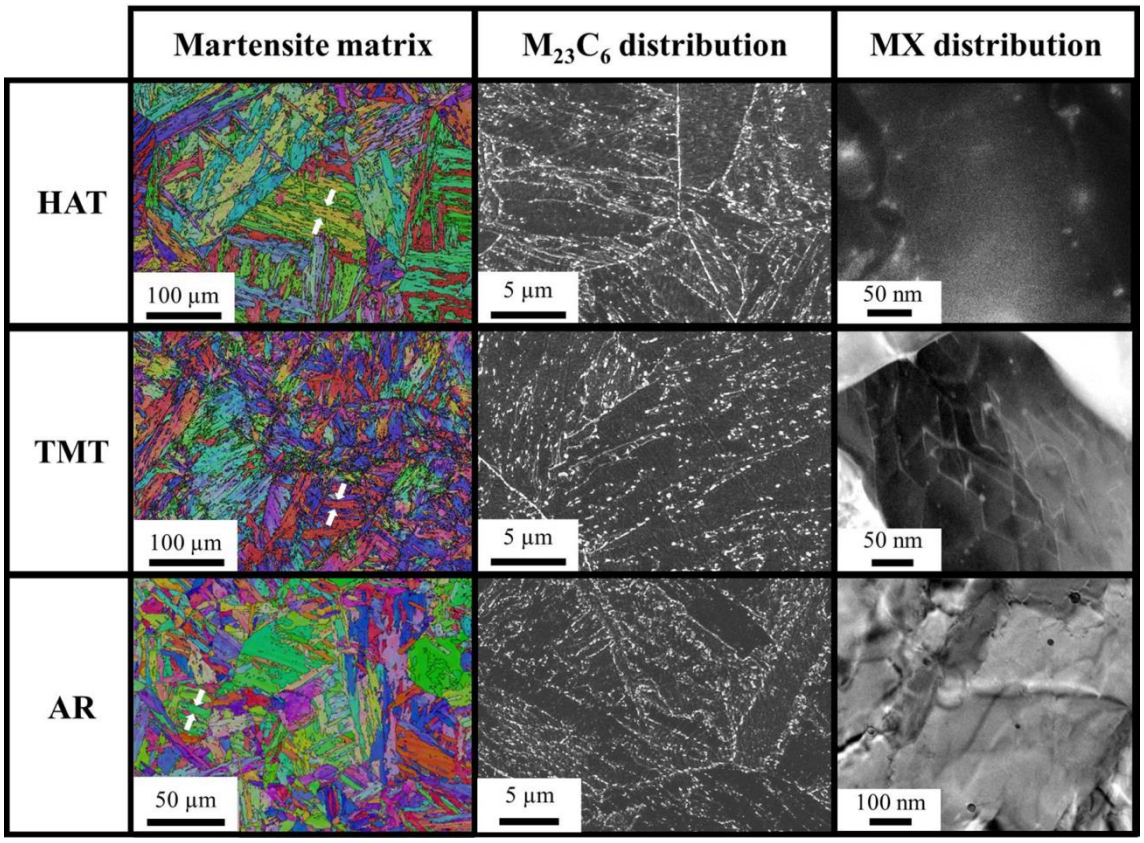

Figure 2. Martensite matrix (martensite block are indicated by white arrows), $M_{23}C_6$ precipitates and MX nanoprecipitates distributions after the different thermomechanical and heat treatments.

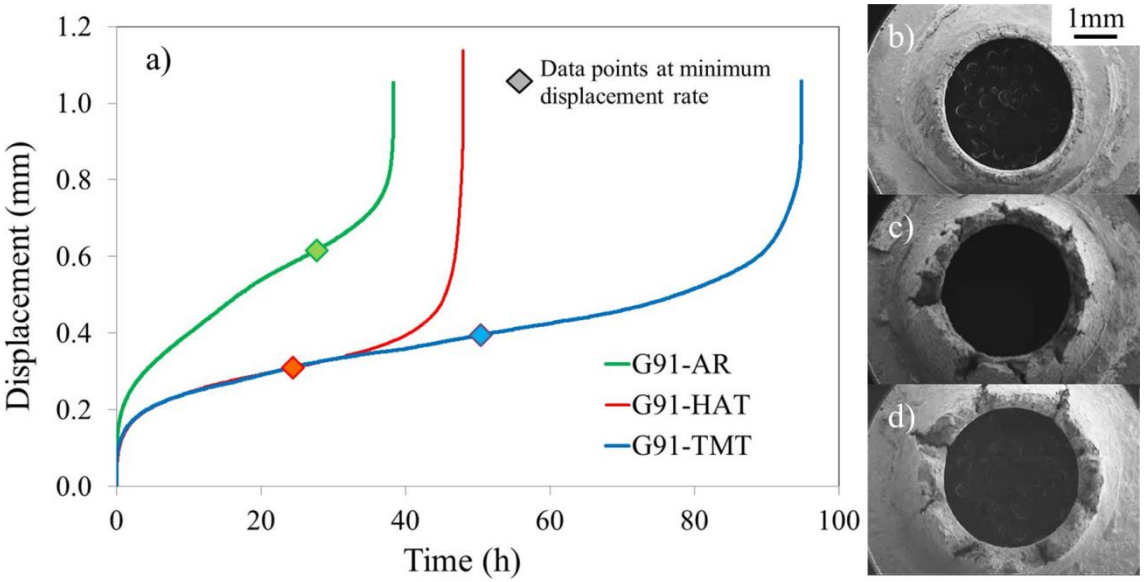

Figure 3 a) SPCT curves measured for the samples after the different thermomechanical and heat treatments and the creep fracture surfaces for the b) AR, c) HAT and d) TMT.